Lateral organization of complex lipid mixtures from multiscale modeling

Paul W. Tumaneng,[1,a)] Sagar A. Pandit,[2] Guijun Zhao,[1] and H. L. Scott[1]
[1]*Department of Biological, Chemical and Physical Sciences and Center for the Molecular Study of Condensed Soft Matter, Illinois Institute of Technology, Chicago, Illinois 60616, USA*
[2]*Department of Physics, University of South Florida, Tampa, Florida 33620, USA*

(Received 13 November 2009; accepted 20 January 2010; published online 12 February 2010)

The organizational properties of complex lipid mixtures can give rise to functionally important structures in cell membranes. In model membranes, ternary lipid-cholesterol (CHOL) mixtures are often used as representative systems to investigate the formation and stabilization of localized structural domains ("rafts"). In this work, we describe a self-consistent mean-field model that builds on molecular dynamics simulations to incorporate multiple lipid components and to investigate the lateral organization of such mixtures. The model predictions reveal regions of bimodal order on ternary plots that are in good agreement with experiment. Specifically, we have applied the model to ternary mixtures composed of dioleoylphosphatidylcholine:18:0 sphingomyelin:CHOL. This work provides insight into the specific intermolecular interactions that drive the formation of localized domains in these mixtures. The model makes use of molecular dynamics simulations to extract interaction parameters and to provide chain configuration order parameter libraries.
 [doi:10.1063/1.3314729]

I. INTRODUCTION

Cell membranes are composed of a variety of amphipathic molecules such as phospholipids and sphingolipids. These lipids form a bilayer structure in the presence of water, where the hydrophilic headgroups are solvated in water and the hydrophobic hydrocarbon chains (henceforth referred to as chains) form the core to minimize contact with water. Bilayer sheets further fold into large scale vesicles to avoid hydrocarbon water contact. The resulting lipid vesicles exhibit complex structural and organizational changes with respect to temperature and lipid concentration, and numerous experimental studies over the past decade have underscored their importance in cellular behavior.

Typical single-component lipid bilayers undergo a first order phase transition from a gel phase, S_o, to a liquid disordered phase, L_α, at a particular melting temperature. As a consequence, some binary mixtures consisting of a lipid with a low melting temperature and a lipid with a high melting temperature exhibit separated regions of L_α and S_o phases, at temperatures intermediate to their respective melting points.[1,2] A recent study of binary phospholipid mixtures[3] has concluded that these domains represent stable thermodynamic phases. However, the mixture studied in Ref. 3 lacks the biologically important presence of cholesterol (CHOL) and sphingolipids.

CHOL has the effect of inducing order in lipid chains to form a liquid ordered, L_o phase, characterized by highly mobile chains that are also well ordered. When CHOL is added to binary mixtures of lipids in bilayers, laterally separated liquid domains consisting of CHOL-rich L_o, and CHOL-depleted L_α regions are observed in experiments.[4,5] These liquid domains form the basis for the concept of "lipid rafts" that are believed to exist in biological plasma membranes[6–9] and are implicated in a number of biologically important cellular functions (see, e.g., Refs. 10 and 11).

The effect of CHOL on the ordering of chains is thought to arise from the structure of the CHOL itself[12,13] and the chains with which the CHOLs interact.[14–21] The rigid CHOL ring structure enforces a tighter packing and reduces the conformational freedom of neighboring lipid chains. CHOL shows a unique level of specificity in inducing order due to *the two faces of the CHOL rings*. That is, the two sides of the CHOL rings are structurally distinct, viz., one face has protruding methyl groups (rough β face), while the other does not (smooth α face). Molecular dynamics simulations[12,13,22] show that lipids having ordered chains due to the lack of unsaturated bonds, tend to pack better with the α face, leaving the lipids with disordered chains to associate more with the β face. Experimentally, the presence of CHOL has been shown to promote lateral inhomogeneity in mixed lipid bilayers,[23] suggesting a role for this anisotropic CHOL-lipid interaction in domain formation. Experiments provide a large body of evidence that model bilayers composed of ternary lipid-CHOL mixtures can indeed segregate into coexisting lateral domains of differing composition[4,5,21,24–29] and that CHOL plays a crucial role in the domain partitioning.

A concrete understanding of specific interactions in lipid-CHOL systems is crucial in unraveling the role of "raftlike" domains in cellular processes.[10,11] To this end, we consider here a system consisting of dioleoylphosphatidylcholine (DOPC) (the low melting point lipid) mixed with 18:0 sphingomyelin (SM) (the high melting point lipid), at various concentrations of CHOL. This system and others like it have been extensively studied experimentally.[1,2,14,24,25,28,30–50] Several ternary phase diagrams have been published, indicating regions where phase separated domains are found. However, to infer the specific

a)Electronic mail: ptumanen@iit.edu.

interactions of lipids and CHOL that are responsible for the observed behavior, we have to resort to modeling efforts.

A number of theoretical and computational modeling efforts have been published in an attempt to study lipid bilayers and interactions of lipid bilayers with CHOL.[51–59] Some of the modeling effort has been centered on thermodynamical construction of phemenological free energy functions,[51–53] while a full statistical mechanical approach has been described by Elliott *et al.*[60,61] They have addressed the role of CHOL and lipids on the lateral organization of model bilayers employing atomistic level self-consistent mean-field theory (SCMFT). The model is utilized to construct ternary phase diagrams of CHOL-lipid mixtures based on a microscopic, phenomenological description of chain ordering as a function of membrane depth. Equilibrium statistical mechanical analysis of the model leads to several different phase diagrams for varying choices of the interaction parameters.

A coarse-grained computational approach based on MD simulations, by Risselada and Marrink,[62] also explores the heterogeneous nature of model membranes. They have employed the Martini model[63] force field to simulate the formation of domains in systems with saturated chain lipids, unsaturated chain lipids, and CHOL. This model removes a large number of degrees of freedom by combining multiple atomic interactions into single interaction centers. Even within this approximation, the emergence of domains is apparent after just a few microseconds. In this paper, we also use a molecular dynamics (MD)-based coarse-graining approach to map the lateral behavior of lipids and CHOL in ternary mixtures, over a wide range of concentrations.

Any model that is aimed at studying the lateral reorganization of lipids has to incorporate time and length scales that greatly exceed those attainable in atomistic MD simulations. Thus, here we extend a coarse-grained SCMFT model, applied earlier to lipid-CHOL binary mixtures,[22,64] and with input from atomistic MD simulations. With this approach, we propagate the MD-generated results into more biologically relevant time and length scales in a three-component mixture. As demonstrated below, we are able to reproduce complex levels of lateral organization, including separated regions with differing chain order and concentration, observed in experiments. The temporal evolution of the local order in this model is calculated similarly to the model of Peng *et al.*[65] in which self-organization is driven by local free energy gradients. Our model differs from the model of Peng *et al.*,[65] in that the mean field free energy of the lipid bilayer is calculated following a model proposed by Marčelja,[22,64,66] specifically designed for lipid bilayer ordering. The Marčelja model (based on liquid-crystal theory) utilizes order-order pairwise interactions between chains and was originally applied with a high degree of success to pure dipalmitoyl phosphatidylcholine (DPPC) in 1974.[66] In a more recent application of the same basic model to DPPC-CHOL mixtures by Scott and co-workers,[22,64] both the lateral organizational properties and the heat capacities of these mixtures were calculated and found to be in excellent agreement with experiment.[67,68]

II. THE SCMFT MODEL

In our model, a leaflet of a lipid bilayer is mapped onto a two-dimensional field of lipid chain order through which CHOL molecules, mapped onto two-dimensional hard rods, may diffuse. For the computational implementation, the field is discretized onto a square lattice. The salient quantity for intermolecular interactions is the scaled chain-averaged molecular order parameter for a single chain:

$$s(\vec{r}) = -\frac{n_{tr}}{n_s}\sum_{m=1}^{n_s}\left(\frac{3}{2}\cos^2\beta_m - \frac{1}{2}\right)/n_s, \tag{1}$$

where n_{tr}/n_s represents the fraction of dihedrals in a trans configuration (n_{tr}) in a single chain to the number of dihedrals along that chain (n_s). β_m is the angle between the normal to the plane defined by the C–H bond vectors and the bilayer normal for carbon m for the chain at the position $\vec{r}$. The form of Eq. (1) differs from previous models such as those due to Elliott *et al.*[60,61] in that we are averaging over the entire chain, rather than treating components of the chain individually. Following the model of Peng *et al.*[65] and our earlier work,[22,64] we introduce CHOL molecules as rigid two-dimensional rods that diffuse over the two-dimensional field and interact locally with the lipid through the field values.

The system Hamiltonian includes order parameter-dependent interactions between neighboring lipid chains, CHOL-lipid chain pairs and CHOL-CHOL neighboring pairs,

$$H_{\text{tot}} = H_{\text{lip-lip}} + H_{\text{lip-CHOL}} + H_{\text{CHOL-CHOL}}. \tag{2}$$

The first term in the Hamiltonian represents interactions between lipid chains:

$$H_{\text{lip-lip}} = -\sum_{\langle ij\rangle} V_0(c)s_i s_j - \sum_{i=1}^{n_{\text{lip}}} V_1(c)s_i\psi_i - \sum_{\langle ij\rangle} V_2(c)\psi_i\psi_j, \tag{3}$$

where sums are over lattice sites and angled brackets indicate sums over nearest neighbors, i,j. In Eq. (3), s_i is the lipid order at lattice site i as defined in Eq. (1) and ψ_i is the relative compositional makeup at site i. That is, in order to accommodate binary lipid DOPC-SM mixtures in the model, we introduce the concentration field $\psi_i = c_{\text{SM},i} - c_{\text{DOPC},i}$, defined as the difference in relative localized concentrations of the two lipid components at site i. The total concentration of SM in the system, which is conserved throughout the simulation, is denoted by $c = 1 - (1/n_{\text{lip}})\sum_{i=1}^{n_{\text{lip}}} c_{\text{DOPC},i}$. The parameters $V_0(c)$, $V_1(c)$, and $V_2(c)$ are concentration dependent coupling constants that model pairwise interactions between lipid molecules as bilinear products of order parameters, order parameter and local concentration, and local concentration fields, respectively. Below we elaborate on the method by which we use MD trajectories to estimate values for the coupling constants and how the time evolution of the concentration field is modeled. Then, in subsequent paragraphs we describe the lipid-CHOL, and CHOL-CHOL terms in Eq. (2).

A. Coupling constants

The interaction constants in Eq. (3) represent interaction energies that are coupled to local order parameters ($V_0(c)$), to local concentration ($V_2(c)$), and to local order-concentration values ($V_1(c)$). As a first approximation, the coupling constants are computed by taking convex combinations of coupling constants of respective pure systems, such as $V_0(c) = V_0^{\mathrm{SM}}c + V_0^{\mathrm{DOPC}}(1-c)$, where V_0^{SM} and V_0^{DOPC} are the coupling constants of systems pure in SM and DOPC, respectively. $V_1(c)$ and $V_2(c)$ have the same concentration dependence.

The parameters $V_0(c)$, $V_1(c)$, and $V_2(c)$ are obtained from analysis of the distributions of intermolecular energies for different order parameter values, in MD simulations. In this procedure, MD trajectories are analyzed to obtain the MD-averaged nearest neighbor pairwise chain energy states as functions of chain order and concentration. A linear fit then yields the relevant coupling constant. The data are, as expected, quite noisy so that the resulting values represent a range of possible coupling constants. However, we have made only one additional modification to the linear fitting results for the lipid-lipid order parameter coupling constant: V_0^{SM} and V_0^{DOPC} were further tuned for each lipid so that the main-chain phase transition temperature is consistent with the experimental value, and this represents the only phenomenological component of this work. This modification generally changed the MD-based values of V_0^{SM} and V_0^{DOPC} by 10%–20%. The coupling between order parameter and concentration field, parameterized by $V_1(c)$, is approximated by analyzing the difference in the product of the intrachain energies and their respective order parameters for both SM chains and DOPC chains. The result is that more highly ordered chains are energetically favored when a higher concentration field is present and vice versa for DOPC chains. The third term in Eq. (3), parameterized by $V_2(c)$, drives formation of domains through differences in interchain interaction strengths for the two lipid types SM and DOPC, as this term energetically favors neighboring lattice sites with similar values in ψ. Analysis of energies due to Lennard-Jones interactions calculated from MD simulation trajectories of SM and DOPC bilayers reveal that intrachain energies due to all the carbons along a chain interacting with each other are typically attractive and greater in magnitude in SM chains than in DOPC chains. The same was true for interchain energies between all carbons along a chain interacting with all carbons along an adjacent chain. As an example, consider two neighboring sites i and j that have a concentration field value representing pure SM ($\psi_i=\psi_j=+1$) or pure DOPC ($\psi_i=\psi_j=-1$). The product of ψ_i and ψ_j is positive in both cases, providing a contribution of $-V_2(c)$ to the energy. If one site has a concentration field value representing pure SM ($\psi_i=+1$) while the other has a value representing pure DOPC ($\psi_j=-1$), the product is negative, providing a contribution of $+V_2(c)$ to the energy. In general, ψ_i can vary continuously between 0 and 1, but the energy preference for same-sign neighbors holds.

B. Concentration field

The presence of two species of lipid in the model at any given lattice site is described by the concentration field $\psi_i = c_{\mathrm{SM},i} - c_{\mathrm{DOPC},i}$ at a site i on the lattice grid. Therefore, each localized point in the two-dimensional model is assigned two field values; an order parameter field value and a concentration field value. Note that the while the fractional lipid concentration can vary at the local level, the overall fractions of these lipids in the system (c_{SM} and c_{DOPC}) remain constant. The field values range continuously from -1 to $+1$ ($c_{\mathrm{SM},i}$ and $c_{\mathrm{DOPC},i}$ each can vary between 0 and 1), with -1 representing pure DOPC and $+1$ representing pure SM. In our model, we evolve the local concentration field through a Cahn–Hilliard equation that relates the time evolution of the local concentration field to changes in the local free energy,[69]

$$\frac{\partial \psi_i}{\partial t} = \Gamma \nabla^2 \frac{\partial F}{\partial \psi_i} + \gamma_i, \tag{4}$$

where F is the free energy, Γ is a lipid mobility parameter, and γ_i is a stochastic noise component. This equation ensures that, while local lipid concentration field values may vary in time, the total lipid concentrations in the system are conserved.

C. Lipid-CHOL and CHOL-CHOL interactions

CHOL molecules are mapped onto the lattice as two-dimensional hard rods that diffuse through the order parameter and concentration fields, as in our earlier work.[22,64] Based on a preponderance of experimental evidence that CHOL primarily affects lipid chain order, the hard rods are assumed to interact locally with the lipid order field only, and with other CHOLs. The second term in the Hamiltonian represents lipid-CHOL interactions and is designed to take into account the asymmetry of the CHOL molecule,

$$H_{\text{lip-CHOL}} = -\sum_{i=1}^{n_{\mathrm{lip}}} \sum_{j=1}^{n_{\mathrm{CHOL}}} V_{\text{lip-CHOL}}(1 - \Delta \sin \theta_{i,j}) s_i. \tag{5}$$

The sums are over all lipid chains and nearby CHOL molecules. The coupling constant, $V_{\text{lip-CHOL}}$, is found from MD trajectories by linear regression analysis of CHOL-lipid chain interactions as a function of order parameter, as described in previous papers.[22,64] The parameter Δ was introduced in earlier work[22] as a means to incorporate the fact that lipid chains are more energetically attracted to the smooth side of CHOL.[22] Thus, it serves to represent the asymmetry of lipid-CHOL interactions in the x-y plane of the bilayer. Each CHOL "rod" has a body coordinate system with a y' axis along the length of the rod starting at the center of mass, and an x' axis extending from the center of mass in the direction perpendicular to the rod on the "rough" side. $\theta_{i,j}$ is defined as the angle between the y' axis of CHOL i and vector connecting the center of mass of CHOL i and the position of lipid j on the lattice.[22] Numerical values for $V_{\text{lip-CHOL}}$ and Δ are the same as used earlier in Ref. 22. We emphasize that Eq. (5) depends only on the local chain order parameter s_i and not on the local value of the concentration field. This is a consequence of our observation in earlier MD

simulation work[12] that the MD-calculated pairwise interaction energy distributions between CHOL and SM are indistinguishable from those between CHOL and DOPC. While one could adjust parameters in the model if one wanted to postulate different interactions, that would not be in keeping with our goal to reduce the number of adjustable parameters to a minimum. There is experimental support for our hypothesis that the dominant interactions that drive lateral organization in lipid bilayers are order parameter dependent. Ternary mixtures of DOPC-DPPC-CHOL have a similar phase diagram as DOPC-SM-CHOL (Ref. 5) (see also the review by Feigenson[70]), which suggests that the lipid-CHOL interactions are driven by the order parameter field rather than the concentration field.

The third term in the Hamiltonian, Eq. (2), represents CHOL-CHOL interactions cast onto the two-dimensional bilayer plane,

$$H_{\text{CHOL-CHOL}} = \sum_{i=1}^{n_{\text{CHOL}}} \sum_{j=1}^{n_{\text{CHOL}}} V_{cc}^{r}(r_{ij}) V_{cc}^{\phi}(\phi_{ij}), \tag{6}$$

where sums are taken over all neighboring CHOL molecules. This term has not been altered from the earlier CHOL-lipid modeling.[22,64] As described there, the two terms in the sum account for the radial and angular energy interactions. Here, r_{ij} is the distance between two close CHOLs, with indices i and j and $\phi_{ij}=\phi_i-\phi_j$ is the difference in angle between two close CHOLs. MD simulations indicate that the CHOL-CHOL interaction is of very short range, so in practice, $H_{\text{CHOL-CHOL}}$ is taken to be a simple repulsive potential,

$$V_{cc}^{r} V_{cc}^{\phi} = \begin{cases} \gamma \sin^2(\phi_{ij}), & r_{ij} \le L, \\ 0, & r_{ij} > L, \end{cases}$$

where $\gamma=13k_BT$ and L is the rod length.[22,64]

The diffusion of CHOL molecules over the order parameter and concentration fields is modeled by the following Langevin equations:

$$\frac{\partial \vec{r}_k}{\partial t} = -M_r \frac{\partial F}{\partial \vec{r}_k} + \vec{\eta}_k \tag{7}$$

and

$$\frac{\partial \theta_k}{\partial t} = -M_\theta \frac{\partial F}{\partial \theta_k} + \zeta_k, \tag{8}$$

where η_k and θ_k are stochastic noise components and M_r and M_θ are CHOL mobilities. $\vec{r}_k$ defines the x,y position of the center of the kth CHOL and θ_k is its orientation. η_k and ζ_k are thermal fluctuations modeled as random variables that obey fluctuation-dissipation theorems. M_r and M_θ, the CHOL mobilities, are related to MD-extracted diffusion constant D and the rotational diffusion constant, D_{rot} by $M_r=D/k_BT$ and $M_\theta=D_{\text{rot}}/k_BT$.[22,64]

D. Mean field modeling method

In the statistical mechanical treatment, we start with the expression for the total partition function for a given distribution of CHOLs,

$$Z_{\text{tot}} = \sum_{i=1}^{n_{\text{lip}}} \sum_{\text{allconfs}} \exp\left[-\frac{H_{\text{tot}}}{k_bT}\right], \tag{9}$$

where H_{tot} is described above. The first sum is over all SM and DOPC chains in the system. The second sum is over all possible configurations of each chain. The possible configurations are enumerated in libraries of order parameter [Eq. (1)] values obtained from MD trajectories as described in earlier work.[22,64] The use of MD libraries allows us to sample the most likely configurations in a bilayer environment, ignoring the extremely large number of conformations that are highly unlikely to be present in a lipid bilayer.

In the self-consistent mean-field approximation, the lipid chain at each lattice site i interacts with a mean field due to neighboring lipids, the number of nearby CHOLs, c_i, and the concentration field,

$$\Phi_i = \sum_{j=1}^{\nu} V_o \langle s_j \rangle + c_i V_{\text{lip-CHOL}} + V_1(c)\psi_i, \tag{10}$$

where ν is the coordination number ($\nu=4$ for a square lattice). This allows us to express the partition function for a single chain as a sum over all possible chain configurations,

$$Z_i = \sum_{\text{allconf}} \exp[\beta \Phi_i s_i]. \tag{11}$$

The usual statistical mechanical treatment results in coupled self-consistent equations for $\langle s_i \rangle$,

$$\langle s_i \rangle = \frac{\Sigma_{\text{allconf}} s_c \exp[\beta \Phi_i s_c]}{\Sigma_{\text{allconf}} \exp[\beta \Phi_i s_c]}. \tag{12}$$

This system of equations is solved iteratively at each time step to find the mean order parameter field.

At each time step, CHOL positions and orientations are propagated according to Eqs. (7) and (8) and the concentration field is propagated according to Eq. (4). Then the self-consistent Eq. (12) is solved. Following this, the mean-field free energy is calculated as

$$F = \sum_{i=1}^{n_{\text{lip}}} [\langle s_i \rangle \Phi_i - k_bT \ln Z_i] + H_{\text{CHOL-CHOL}} - \frac{1}{2} \sum_{i=1}^{n_{\text{lip}}} \sum_{j=1}^{\nu} V_2(c) \psi_i \psi_j, \tag{13}$$

which is used to update the Langevin Eqs. (7) and (8) and the Cahn–Hilliard Eq. (4) for the next time step. This completes one time step and the steps after initialization are repeated until microsecond times are reached.

III. APPLICATION TO DOPC-SM-CHOL MIXTURES

Each simulation was initialized with random distributions of both order and concentration fields (at the given lipid concentration ratio), and randomly distributed CHOLs. Simulations were carried out on a 100 by 100 square lattice, which translates to 5000 lipids (10 000 chains) in the DOPC-SM-CHOL system. The phase transition temperatures of DOPC and SM are roughly 253 and 318 K, respectively. We therefore set the temperature for our system at 303 K, where

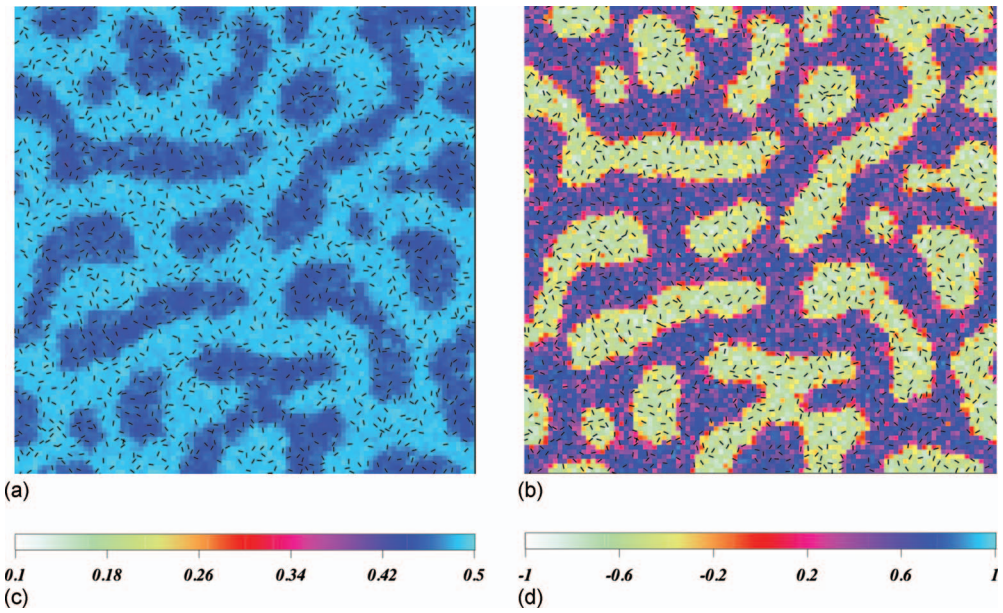

FIG. 1. Trajectory snapshots of order parameter (a) and concentration field (b) for the DOPC:SM:CHOL concentration 35:40:25. CHOLs are visible as small black segments representing the two-dimensional rods. Color codes are in (c) and (d).

domain formation is known to occur. Timesteps were taken at 0.1 ns steps, and all runs reached at least 1 μs. Simulations were run for lipid concentrations varying from 0% to 100% for SM and the phospholipid, and for CHOL concentrations between 0% and 50%.

Lateral organizational behavior was determined at each simulated concentration by analyzing the patterns observed in order parameter and concentration field distribution plots and trajectory snapshots. Typical snapshots of order parameter and concentration field are shown in Fig. 1 for the DOPC:SM:CHOL concentration triplet 35:40:25 after 1 μs of simulation. It is clear from the patterns in the snapshots that regions of higher order parameter correspond to regions of a higher concentration of SM and regions of lower order parameter correspond to regions of a higher concentration of DOPC. CHOLs in Figs. 1(a) and 1(b) are represented by short black lines. A narrow transition region is found along the boundaries in Figs. 1(a) and 1(b). The order parameter trajectory snapshot in Fig. 1(a) shows dark blue regions representing lower order parameter values and light blue regions representing higher order parameter values. In the concentration field plot in Fig. 1(b), the pattern shows SM-rich concentrations (dark) separated from DOPC-rich concentrations (light). Distributions of order parameter and concentration field values are shown in Figs. 2(a) and 2(b), respectively, and were obtained by separately binning order parameter and concentration field values from each lattice site. The bimodality of the high and relatively high peaks in concentration and order shown in Fig. 2. In the concentration field distribution [Fig. 2(b)], there are two separate peaks corresponding to regions of the field rich in SM and DOPC, respectively. In the order parameter field [Fig. 2(a)], the peaks are quite close and overlap, indicating a high degree of order for both SM and DOPC at 25% CHOL.

We can distinguish regions on a ternary phase plot[71] by the presence or absence of bimodality in distributions of order and concentration fields. The locations of these regions can then be compared with experimental plots.[4] We find a very good match between experiment and model results in terms of the structure of the lateral organizations at different points on the ternary diagrams. Figure 3 illustrates this comparison for DOPC:SM:CHOL mixtures. Figure 3(a) shows an experimental diagram[4] with superimposed arrows that in-

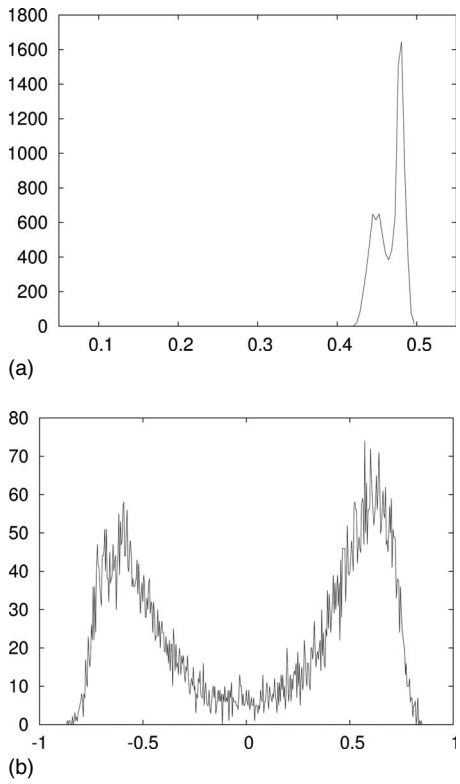

FIG. 2. Distributions of order parameter (a) and concentration field (b) for the DOPC:SM:CHOL concentration 35:40:25.

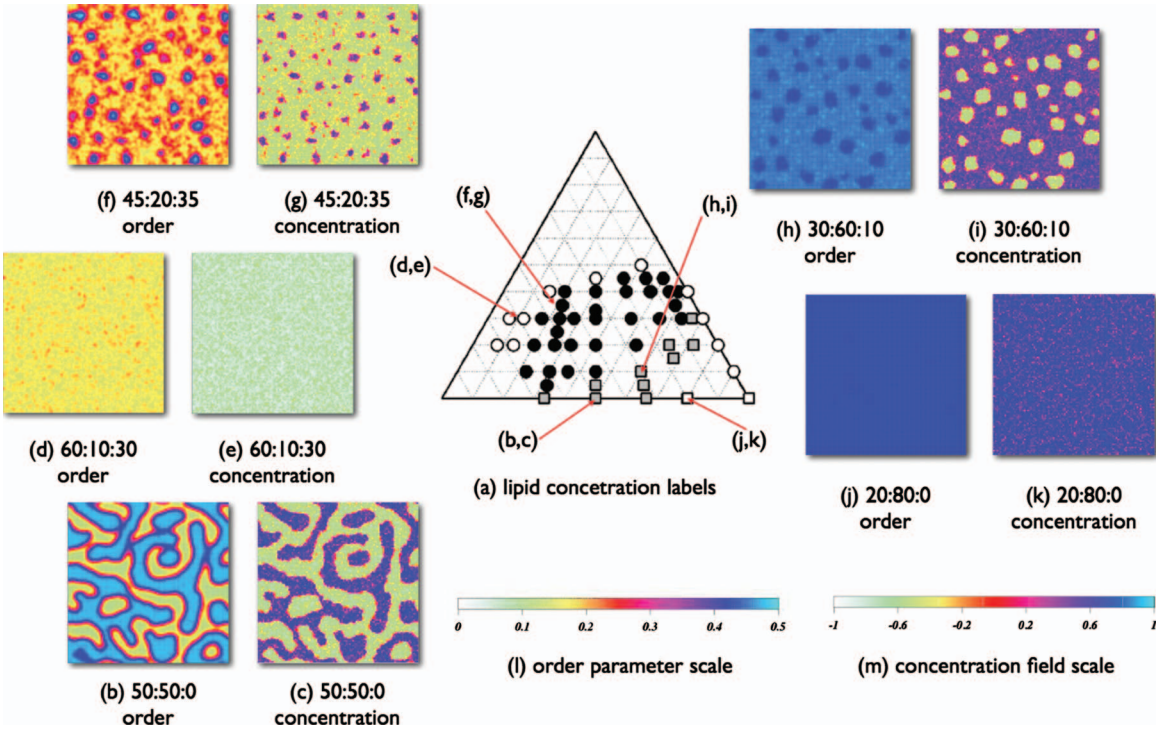

FIG. 3. (a)Experimentally derived phase plot from Veatch and Keller (Ref. 4). Black, white, and gray squares and circles are experimental points. White circles represent concentrations consisting of a uniform liquid phase, black circles denote coexisting liquid phases, gray squares denote coexisting gel, and liquid phases and white squares represent a uniform gel phase. Superimposed over the experimental plot are labels marking positions on the diagram that correspond to simulated DOPC:SM:CHOL order parameter plots shown in (b)–(k). At each represented concentration, order parameter field and the concentration field snapshots after 1 μs are shown. CHOLs have been removed for clarity. The patterns reveal a separation into domains that is present in both fields at some concentrations. The scale of order parameter is shown in (l) and the scale of concentration field is shown in (m). The similarities between experiment and simulation are discussed in the text.

dicate simulated concentrations. We display order parameter and concentration fields that we have simulated at those points in Figs. 3(b)–3(k).

In Figs. 3(b) and 3(c), we show the snapshots of order parameter and concentration fields for the DOPC:SM:CHOL triplet 50:50:0. There is clear separation between a high and low value of order parameter. Additionally, the separation into domains occurs at the same regions on the concentration field plot. The domains consisting of higher value of order parameter are rich in SM and the domains consisting of lower value of order parameter are rich in DOPC. This is very similar to the points in the experimental plot near that concentration, represented by a gray square, where a gel phase is in coexistence with a liquid phase.

In Figs. 3(d) and 3(e), we find no clear separation in order parameter and concentration field, respectively, but it is clear that the presence of CHOL results in enhanced ordering of chains to chain-averaged values near 0.2, compared to about 0.1–0.15 for fluid phase DOPC. This ordering of chains is seen in the color variations in Fig. 2(c) that show no long range order. This point is directly comparable to the analogous phase region indicated by the arrow (d,e) on the experimental phase diagram, and represented by an open circle, indicating a phase in which no lipid domains are observed.

In Figs. 3(f) and 3(g), representing 35% CHOL and 45:20 DOPC:SM concentration, there are separated regions of a low and high order parameter and concentration field. Low and high order parameters are also seen in the areas surrounding this point on the experimental diagram, indicated by the arrow labeled (f,g) and are identified by Veatch and Keller as coexisting liquid ordered and liquid disordered regions.

In Figs. 3(h) and 3(i), the plots representing 30:60:10 with a larger concentration of SM, we observe a region of high order and a region of intermediate order. The corresponding experimental point on the phase diagram is represented by a gray square, indicating that there is a coexistence between a gel and liquid phase. At high degrees of lipid order (average chain order around 0.4) the differences between the two bimodal regions is more subtle, and represents a coexistence between a "gel-like" phase (so labeled because peak order parameter values are closer to 0.5) and liquid ordered regions (peak order parameter values closer to 0.4). Experimental data seem to indicate the coexistence of a gel phase and a liquid disordered phase, at least near the point labeled (h,i), which is consistent with the bimodal concentration field seen in Fig. 3(i).

Finally, Figs. 3(j) and 3(k) show a homogeneous system with order parameter and concentration fields that vary little spatially. The points on the experimental diagram around this point, labeled (j,k), have white squares that represent a single region of gel-like order. We point out that in all cases, model domains are much smaller than the micron-sized patterns seen in experiment, but this is a consequence of the much smaller scale of the model, compared to the micron-sized experimental vesicles, and to the difference in time scales.

A ternary plot, constructed from order parameter distri-

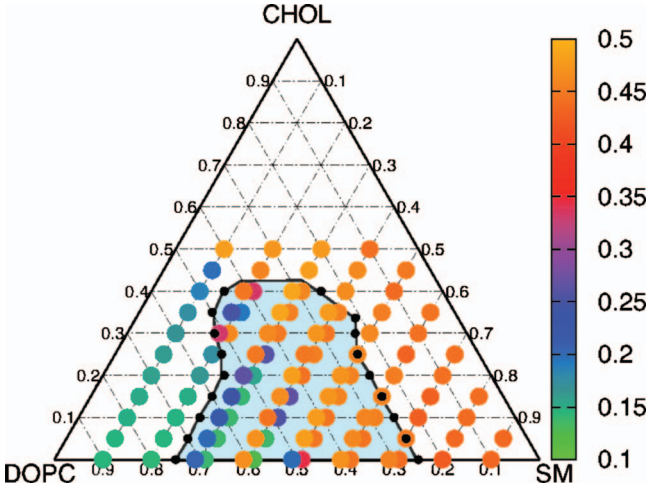

FIG. 4. DOPC-SM-CHOL ternary lateral organization diagram. The shaded region indicates the presence of bimodality in the order parameter distributions. Dots indicate the average order parameter values, with coloring represented by the key to the right. Two overlapping dots that appear in the bimodal region represent the average order parameter of each peak.

butions, is shown in Fig. 4. The dots represent the average value of order parameter at the peaks of each distribution. Regions of bimodality are given the two dots shown, representing the values of order. In this figure, we have drawn a boundary contour within which our simulations indicate the presence of bimodality in lipid order and concentration. The boundary defining this region is approximated by fitting the peaks to Gaussian curves and interpolating where the area under these curves would become zero. The resolution of this boundary is limited by the number of simulations carried out.

The colored dots in Fig. 4 representing peaks in order parameter distribution tend to shift continuously as concentration is adjusted. As an example, consider the peaks along the 20% CHOL concentration line. Toward the right of the diagram, a single peak is present in the order distribution with a relatively high value. Moving toward the left along the 20% CHOL concentration line, we traverse the line that separates the region of bimodality from the single peak region. In here, a second peak in the distribution appears. Moving further to the left within the bimodality region, both curves shift to lower order values until the coexistence line is traversed again and only a single peak remains at a relatively low value of order. Thus, as one moves laterally around the ternary plot, the order parameter peaks shift and at certain points on the diagram, the bimodality in peaks is reminiscent of laterally segregated phases seen in experiment, as described in paragraphs above. Because the peaks shift continuously as concentration is changed, it is not possible to use lipid chain averaged order to delineate specific portions of the ternary diagram at which various phases can be represented. However we note that, based on order parameter values, we can assign standard phase nomenclature to the various points in Fig. 4, specifically the bimodal regions: orange-orange dot pairs represent gel-like and L_o; orange-green/lavender dot pairs represent L_α and L_o; blue-green dot pairs represent bimodality in which both distributions have peaks at relatively low values for the order parameter. We interpret the latter as a gradual lowering of the L_o (orange to lavender) order as DOPC concentration increases.

While the changes in order parameter are subtle and involve the appearance and disappearance of shoulders on the distributions of chain order, and as used for the construction of Fig. 4, bimodality in the concentration field has a different nature. Figure 2(b) shows two distinct and nonoverlapping concentration regions for an equimolar mixture of SM and DOPC at 25% CHOL. To further illustrate the nature of the changes in order and concentration, we show in Fig. 5 a series of plots of both fields at 20% CHOL for all lipid mixtures studied in the simulations. This figure clearly shows the changes in the concentration field as a single peak at high DOPC levels, evolving into two separate peaks as the concentrations become closer to equimolar, and then evolving back into a single peak as the concentration approaches high SM levels (or vice versa). As discussed above, changes in the distribution of the order parameter field generally follow those of the concentration field but the differences in the latter case are smaller and occur as shoulders on the distribution plots rather than as separate peaks. This property of the order parameter distributions as compared to the concentration distributions is due to the combined effect of chain-CHOL and chain-chain interactions. While all lipid chains are affected by the presence of CHOL, they are also affected by the presence of other lipid chains. That is, at high SM concentration, the relatively high values of the chain order parameters for that lipid will have the affect of ordering the minority DOPC chains, and vice versa for high DOPC concentration. Figures 5(g) and 5(h) show equimolar mixtures of DOPC and SM, plus 20% CHOL. So for this mixture DOPC is ordered both by CHOL and by SM. Decreasing the SM concentration by 10% [Figs. 5(i) and 5(j)] or increasing the SM concentration by 10% [Figs. 5(e) and 5(f)] cause large shifts to the left or right, respectively, in the concentration distributions. The order distribution becomes broader and shifts to much lower values when the DOPC concentration is raised [Fig. 5(g)] and becomes sharper as the SM concentration is raised [Fig. 5(e)]. These trends are consistent with a complex system where chain ordering is strongly dependent on the composition of the mixture, due to both chain-chain and chain-CHOL interactions. The trends are also supported by a large atomistic MD simulation of a single central domain containing both SM and CHOL molecules, that was surrounded by DOPC molecules.[72] In this simulation Pandit *et al.*[72] found, using Voroni tesselation, that DOPC molecules within about 5–6 nm of the SM domain had molecular areas of about 60 $Å^2$, compared to 65–70 $Å^2$ in pure fluid DOPC. We also note that our model depicts the results from 1 μs simulations. But this is a fairly short time in an ongoing time evolution of order, and we discuss in the following section the likely effects of much longer simulations under the Cahn–Hilliard equation.

IV. SUMMARY

In summary, we have presented a coarse-grained, dynamic, self-consistent mean-field theoretical model of a biologically important ternary mixture. In this MD-based model

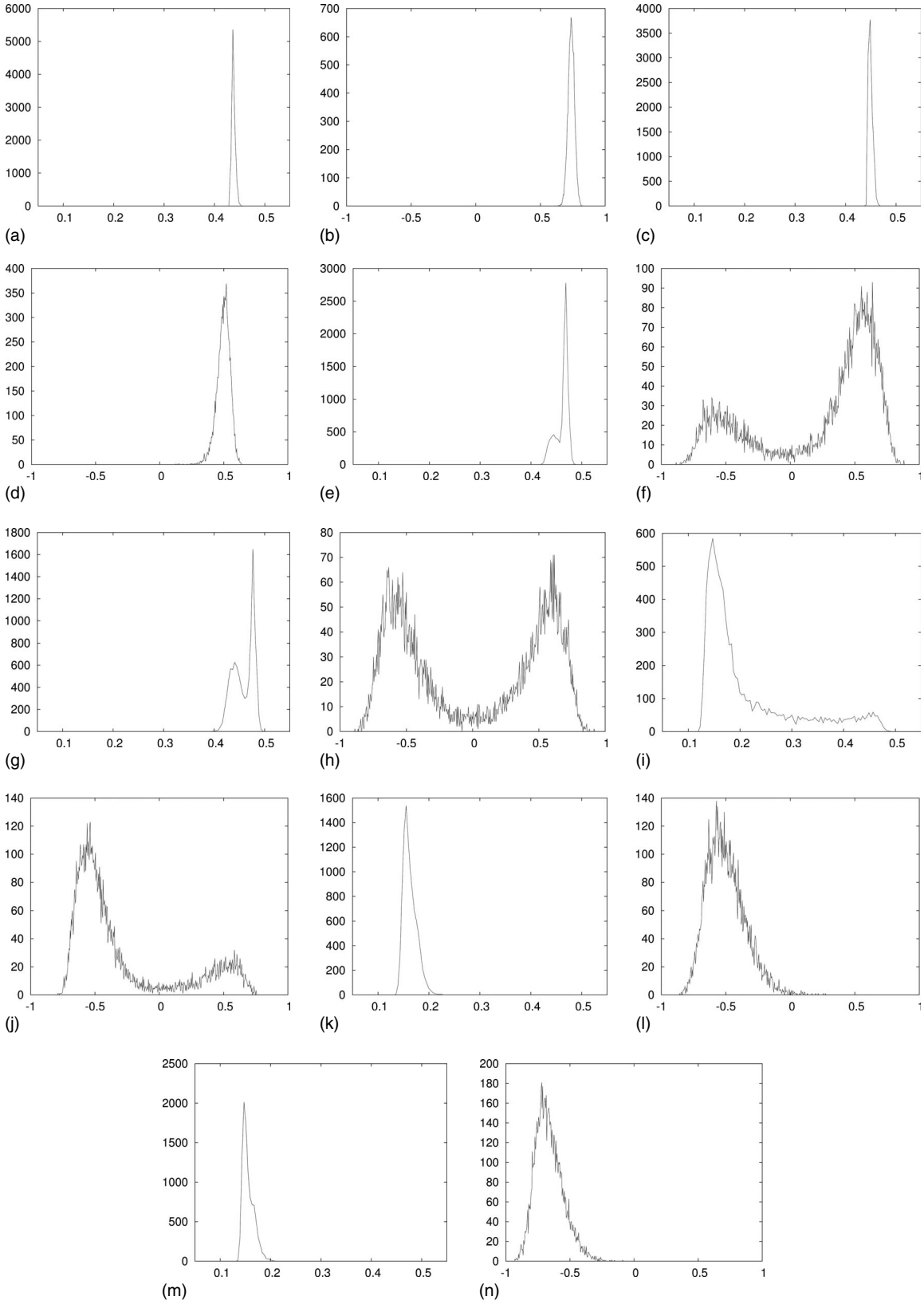

FIG. 5. Distribution plots of order parameter and concentration field for the DOPC:SM:CHOL concentrations labeled for the last snapshot of 1 μs simulations.

of lipid domain formation, input in the form of coupling constant estimates and chain configuration libraries are extracted directly from MD simulation trajectories. The present model differs from the model of Elliot *et al.*[60,61] in that temporal evolution of membrane order and compositional heterogeneity are explicitly modeled, and in that MD data are used in the parameterization process and in building the set of chain configurations. The predictive strength of the model is evident when analogies are drawn between simulation results and experimental treatments of similar systems. In par-

ticular, single- and double-peak order parameter and concentration field distributions reveal patterns that resemble regions on published experimental ternary plots.[4]

Of particular importance is the explicit inclusion of anisotropy in CHOL structure in this model, contained in the parameter Δ in Eq. (5). Equation (5) is, without Δ, similar to the model of Putzel and Schick,[52,53] and could by itself produce model ternary mixtures for a set of values of the coupling constants. However, as we have pointed out in our previous application of this model to a DPPC-CHOL bilayer,[22] the anisotropic nature of CHOL is necessary to produce properties of the system consistent with experiment. In our earlier work,[22,64] it was found that a nonzero Δ was essential to obtain heat capacities and bimodalities that were in close agreement with experiment with DPPC-CHOL mixtures.[67] For this reason, we conclude that, due to the difference between the two "faces" of CHOL, as incorporated through the constant Δ in Eq. (5) above, it is necessary for the formation and distribution of ordered domains that are consistent with experiment.

While the observed bimodalities in lipid chain order in this model appear and disappear continuously as concentrations vary, mean-field theory in general predicts first order changes in phase as a function of lipid concentration. This general property is consistent with the observed pattern of concentration field bimodality in Fig. 5. Since changes in chain order are more closely related to experimental fluorescence measurements, we note that we find here, and also found in our DPPC-CHOL work,[22,64] that above a CHOL concentration of about 5% (the lowest nonzero CHOL concentration modeled), changes in *chain order* evolve continuously, at least in the time and length scales of the simulation. For the present ternary model, as one approaches the bimodal region (shaded region in Fig. 4) a single peak in the distribution of order over the model evolves into a peak with a shoulder that eventually separates fully or partially from the original peak, giving two separated regions of order over the lattice. However, at higher CHOL concentration the two peaks can be quite close together (orange-orange for example, in Fig. 4) with nonvanishing overlap. Leaving the bimodal region, the two peaks in order blend into a single peak. Experimentally, and consistent with the Gibbs Phase Rule, regions of three-phase coexistence are often found in ternary mixtures of the type considered here. While we do not observe any clear trimodality in the order parameter distributions at any simulated concentrations, there are regions where the calculated distributions of order and concentration are broad and noisy [for example Figs. 5(i) and 5(j)], so that longer simulations might reveal subtle third peaks. Further resolution of the peak structure over time and over concentration changes would require significantly more, larger, and longer simulations than have been done here. It is important to note that this model continues to evolve in time, and that in general the domains in this model, and others based on the Cahn–Hilliard equation, grow slowly in size over time,[73] so that another order of magnitude increase in the simulation time could produce wider variation and higher resolution in the order parameter distributions.

The model can be extended to virtually any ternary mixture consisting of two lipids and CHOL if the appropriate MD libraries are constructed and trajectories analyzed for coupling constants. In ongoing work, a similar treatment for palmitoy-oleoyl phosphatidylcholine, with both an unsaturated and a saturated chain, mixed with palmitoyl sphingomyelin and CHOL, is in progress. This work, to be published elsewhere, will address the issue of domain formation associated with this level of unsaturation and will treat the asymmetry of the lipid structure.

ACKNOWLEDGMENTS

We thank Michael Schick, Gerald Feigenson, and the referee for helpful comments and discussions. P.T., G.Z., and H.L.S. are funded by Grant No. PHS 2 PN2 EY016570B from the National Institutes of Health through the NIH Roadmap for Medical Research and Army Research Office Grant No. W911NF-08-2-0058.

[1] R. de Almeida, A. Feorov, and M. Prieto, Biophys. J. **85**, 2406 (2003).
[2] C. K. Haluska, A. P. Schröder, P. Didier, D. Heissler, G. Duportail, Y. Mély, and C. Marques, Biophys. J. **95**, 5737 (2008).
[3] M. Fidorra, A. Garcia, J. H. Ipsen, S. Härtel, and L. A. Bagatolli, Biochim. Biophys. Acta **1788**, 2142 (2009).
[4] S. L. Veatch and S. L. Keller, Phys. Rev. Lett. **94**, 148101 (2005).
[5] S. Veatch and S. Keller, Biophys. J. **85**, 3074 (2003).
[6] K. Jacobson, O. G. Mouritsen, and R. G. W. Anderson, Nat. Cell Biol. **9**, 7 (2007).
[7] D. Marsh, Biochim. Biophys. Acta **1788**, 2114 (2009).
[8] L. J. Pike, J. Lipid Res. **44**, 655 (2003).
[9] L. J. Pike, Biochem. J. **378**, 281 (2004).
[10] J. Hancock, Nat. Rev. Mol. Cell Biol. **7**, 456 (2006).
[11] K. Simons and E. Ikonen, Nature (London) **387**, 569 (1997).
[12] S. A. Pandit, E. Jakobsson, and H. L. Scott, Biophys. J. **87**, 3312 (2004).
[13] S. A. Pandit, S. Chiu, E. Jakobsson, A. Grama, and H. L. Scott, Langmuir **24**, 6858 (2008).
[14] J. Aittoniemi, P. S. Niemelä, M. T. Hyvönen, M. Karttunen, and I. Vattulainen, Biophys. J. **92**, 1125 (2007).
[15] M. Rappolt, M. F. Vidal, M. Kriechbaum, M. Steinhart, H. Amenitsch, S. Bernstorff, and P. Laggner, Eur. Biophys. J. **31**, 575 (2003).
[16] S.-L. Niu and B. J. Litman, Biophys. J. **83**, 3408 (2002).
[17] H. Heerklotz and A. Tsamaloukas, Biophys. J. **91**, 600 (2006).
[18] B. L. Stottrup and S. L. Keller, Biophys. J. **90**, 3176 (2006).
[19] J. Pan, S. Tristram-Nagle, and J. F. Nagle, Phys. Rev. E **80**, 021931 (2009).
[20] A. Tsamaloukas, H. Szadkowska, and H. Heerklotz, Biophys. J. **90**, 4479 (2006).
[21] T. T. Mills, G. E. S. Toombes, S. Tristram-Nagle, D.-M. Smilgies, G. W. Feigenson, and J. F. Nagle, Biophys. J. **95**, 669 (2008).
[22] S. A. Pandit, G. A. Khelashvili, E. Jakobsson, A. Grama, and H. L. Scott, Biophys. J. **92**, 440 (2007).
[23] M. Ratajczak, E. Chi, S. Frey, K. Cao, L. Luther, K. Kjaer, J. Majewski, and K. Lee, Phys. Rev. Lett. **103**, 028103 (2009).
[24] S. L. Veatch and S. L. Keller, Phys. Rev. Lett. **89**, 268101 (2002).
[25] N. Kahya, D. Scherfeld, K. Bacia, B. Poolman, and P. Schwille, J. Biol. Chem. **278**, 28109 (2003).
[26] G. Feigenson and J. Buboltz, Biophys. J. **80**, 2775 (2001).
[27] B. Ramstedt and J. P. Slotte, Biochim. Biophys. Acta **1758**, 1945 (2006).
[28] K. K. Halling, B. Ramstedt, J. H. Nuström, J. P. Slotte, and T. K. M. Nyholm, Biophys. J. **95**, 3861 (2008).
[29] S. Veatch, K. Gawsrisch, and S. Keller, Biophys. J. **90**, 4428 (2006).
[30] A. Bunge, P. M. Müller, M. Stöckl, A. Herrmann, and D. Huster, Biophys. J. **94**, 2680 (2008).
[31] B. Stottrup, D. Stevens, and S. Keller, Biophys. J. **88**, 269 (2005).
[32] Z. Zhang, S. Y. Bhide, and M. L. Berkowitz, J. Phys. Chem. **111**, 12888 (2007).
[33] A. Pokorny, L. E. Yandek, A. I. Elegbede, A. Hinderliter, and P. F. F. Almeida, Biophys. J. **91**, 2184 (2006).
[34] R. F. M. de Almeida, J. Borst, A. Fedorov, M. Prieto, and A. J. W. G. Visser, Biophys. J. **93**, 539 (2007).

[35] G. Lindblom, G. Orädd, and A. Filippov, Chem. Phys. Lipids **141**, 179 (2006).
[36] J. Zhao, J. Wu, F. A. Heberle, T. T. Mills, P. Klawitter, G. Huang, G. Costanza, and G. W. Feigenson, Biochim. Biophys. Acta **1768**, 2764 (2007).
[37] M. D. Collins and S. L. Keller, Proc. Natl. Acad. Sci. U.S.A. **105**, 124 (2008).
[38] F. A. Heberle, J. T. Buboltz, D. Stringer, and G. W. Feigenson, Biochim. Biophys. Acta **1746**, 186 (2005).
[39] D. J. Moore, R. G. Snyder, M. E. Rerek, and R. Mendelsohn, J. Phys. Chem. **110**, 2378 (2006).
[40] L. Zheng, C. M. McQuaw, A. G. Ewing, and N. Winograd, J. Am. Chem. Soc. **129**, 15730 (2007).
[41] J. Zhao, J. Wu, H. Shao, F. Kong, N. Jain, G. Hunt, and G. Feigenson, Biochim. Biophys. Acta **1768**, 2777 (2007).
[42] A. Filippov, G. Orädd, and G. Lindblom, Biophys. J. **93**, 3182 (2007).
[43] A. Filippov, G. Orädd, and G. Lindblom, Biophys. J. **84**, 3079 (2003).
[44] P. Cicuta, S. L. Keller, and S. L. Veatch, J. Phys. Chem. B **111**, 3328 (2007).
[45] B. M. Castro, R. F. M. de Almeida, L. C. Silva, A. Fedorov, and M. Prieto, Biophys. J. **93**, 1639 (2007).
[46] O. Bakht, P. Pathak, and E. London, Biophys. J. **93**, 4307 (2007).
[47] M. L. Frazier, J. R. Wright, A. Pokorny, and P. F. F. Almeida, Biophys. J. **92**, 2422 (2007).
[48] T. S. Ursell, W. S. Klug, and R. Phillips, Proc. Natl. Acad. Sci. U.S.A **106**, 13301 (2009).
[49] S. L. Veatch, O. Soubias, S. L. Keller, and K. Gawsrisch, Proc. Natl. Acad. Sci. U.S.A. **104**, 17650 (2007).
[50] D. Lichtenberg, F. M. G. Ni, and H. Heerklotz, Trends Biochem. Sci. **30**, 430 (2005).
[51] T. Idema, J. M. J. van Leeuwen, and C. Storm, Phys. Rev. E **80**, 041924 (2009).
[52] G. Garbès Putzel and M. Schick, Biophys. J. **95**, 4756 (2008).
[53] G. G. Putzel and M. Schick, Biophys. J. **96**, 4935 (2009).
[54] D. R. Fattal and A. Ben-Shaul, Biophys. J. **67**, 983 (1994).
[55] A. Ben-Shaul, I. Szleifer, and W. M. Gelbart, J. Chem. Phys. **83**, 3597 (1985).
[56] D. W. R. Gruen, J. Phys. Chem. **89**, 146 (1985).
[57] M. Müller, K. Katsov, and M. Schick, Phys. Rep. **434**, 113 (2006).
[58] H. McConnell, J. Chem. Phys. **130**, 165103 (2009).
[59] Q. Shi and G. A. Voth, Biophys. J. **89**, 2385 (2005).
[60] R. Elliott, I. Szleifer, and M. Schick, Phys. Rev. Lett. **96**, 098101 (2006).
[61] R. Elliott, K. Katsov, M. Schick, and I. Szleifer, J. Chem. Phys. **122**, 044904 (2005).
[62] H. J. Risselada and S. J. Marrink, Proc. Natl. Acad. Sci. U.S.A. **105**, 17367 (2008).
[63] S. J. Marrink, H. J. Risselada, S. Yefimov, D. P. Tieleman, and A. H. deVries, J. Phys. Chem. B **111**, 7812 (2007).
[64] G. A. Khelashvili, S. A. Pandit, and H. L. Scott, J. Chem. Phys. **123**, 034910 (2005).
[65] G. Peng, F. Qiu, V. Ginzburg, D. Jasnow, and A. Balazs, Science **288**, 1802 (2000).
[66] S. Marčelja, Biochim. Biophys. Acta **367**, 156 (1974).
[67] M. R. Vist and J. H. Davis, Biochemistry **29**, 451 (1990).
[68] T. H. Huang, C. W. B. Less, S. K. D. Gupta, A. Blume, and R. G. Griffin, Biochemistry **32**, 13277 (1993).
[69] P. M. Chaiken and T. C. Lubensky, *Principles of Condensed Matter Physics* (Cambridge University Press, Cambridge, 1995).
[70] G. W. Feigenson, Biochim. Biophys. Acta **1788**, 47 (2009).
[71] G. W. Feigenson, Annu. Rev. Biophys. Biomol. Struct. **36**, 63 (2007).
[72] S. A. Pandit, S. Vasudevan, S. W. Chiu, R. J. Mashl, E. Jakobsson, and H. L. Scott, Biophys. J. **87**, 1092 (2004).
[73] J. Zhu, L.-Q. Chen, J. Shen, and V. Tikare, Phys. Rev. E **60**, 3564 (1999).